# Selective Ablation of Xe from Silicon Surfaces: Molecular Dynamics Simulations and Experimental Laser Patterning

Ori Stein,[†] Zhibin Lin,[‡] Leonid V. Zhigilei,[§] and Micha Asscher*,[†]

[†]Institute of Chemistry, The Hebrew University of Jerusalem, Jerusalem 91904, Israel

[‡]Renewable Energy Materials Research Science and Engineering Center Department of Physics, Colorado School of Mines, Golden, Colorado 80401, United States

[§]Department of Materials Science & Engineering, University of Virginia, Charlottesville, Virginia 22904, United States

ABSTRACT: The mechanism of laser-induced removal of Xe overlayers from a Si substrate has been investigated employing MD simulations and evaluated by buffer layer assisted laser patterning experiments. Two distinct regimes of overlayer removal are identified in the simulations of a uniform heating of the Si substrate by a 5 ns laser pulse: The intensive evaporation from the surface of the Xe overlayer and the detachment of the entire Xe overlayer driven by explosive boiling in the vicinity of the hot substrate. Simulations of selective heating of only a fraction of the silicon substrate suggest that the lateral heat transfer and bonding to the unheated, colder regions of the Xe overlayer is very efficient and suppresses the separation of a fraction of the overlayer from the substrate. Interaction with surrounding cold Xe is responsible for significant increase in the substrate temperature required for achieving the spatially selective ablation of the overlayer. The predictions of the MD simulations are found to be in a qualitative agreement with the results of experimental measurements of the threshold laser power required for the removal of Xe overlayers of different thickness and the shapes of metallic stripes generated by buffer-assisted laser patterning.
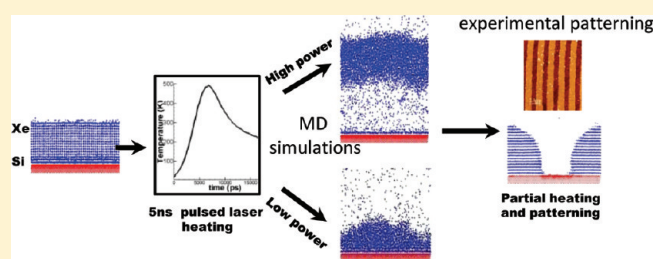
1. INTRODUCTION

The abrupt ejection of a thin molecular or atomic layer adjacent to an absorbing substrate rapidly heated by short pulse laser irradiation is a phenomenon that is used in a variety of applications, ranging from cleaning of semiconductor surfaces from contaminating nanoparticles[1,2] to laser desorption of large biomolecules for mass spectrometry analysis.[3−5] We recently developed a new technique that adopts the concept of laser-induced ejection of a volatile layer for generation of size-controlled arrays of metallic clusters or nanowires.[6−9] In this technique, buffer layer assisted laser patterning (BLALP), a buffer layer of frozen inert gas atoms (e.g., Xe) or volatile molecules (e.g., CO_2 and H_2O) is deposited on a cooled substrate and is exposed to metal atoms evaporated from a hot source, leading to condensation of a thin metal layer or small polyatomic clusters on the surface of the buffer layer. The multilayered system is then irradiated by a short, split laser pulse to create interference pattern on the surface and to selectively ablate stripes of the volatile buffer layer along with the metal adlayer deposited on it. This step is followed by a slow thermal annealing to evaporate the remaining parts of the buffer layer and to soft-land the remaining stripes of the upper layer on the substrate. Thus, the technique combines a method for generation of grating-like surface patterns by laser interference,[10,11] with a buffer-assisted method for fabrication and soft-landing of metal clusters.[12,13]

With a single, low power laser pulse, the BLALP technique has been demonstrated to be capable of producing patterns of

parallel stripes of potassium[6] and gold nanoclusters,[7] as well as continuous gold wires[8] strongly bound to ruthenium substrates. A modified version of the BLALP technique that involves laser patterning of the buffer layer prior to the deposition of the metal layer has also been recently used to generate smooth metallic stripes on metallic[9] as well as oxide $(SiO_2/Si(100))$ substrates. The unique advantage of BLALP is the low laser power needed for patterning, which eliminates damage to the substrate commonly observed in direct laser patterning of metallic layers.

The relevance of the laser-driven ejection of a layer of volatile material from an absorbing substrate for a variety of applications has motivated a number of experimental[14−17] and computational studies[18−24] targeted at revealing the fundamental mechanisms responsible for the layer ejection. The physical picture emerging from these investigations suggests that fast vaporization (or explosive boiling) and expansion of a superheated part of the layer adjacent to the hot substrate provides the driving force for the ejection of the remaining part of the layer. While the highly nonequilibrium nature of the explosive vaporization of the interfacial layer introduces uncertainty to the analytical description of this phenomenon, the atomic-level molecular dynamics (MD)

ACS Publications   © 2011 American Chemical Society

6250

dx.doi.org/10.1021/jp111658w | *J. Phys. Chem. A* 2011, 115, 6250–6259

simulation technique is free from assumptions on the ejection mechanisms and is particularly suitable for the investigation of the processes leading to the ejection of the volatile layer. In particular, MD simulations of the layer lift off from a heated substrate have been performed for a number of systems, including a water ice film deposited on a Au substrate,[19−21] a generic two dimensional fluid−substrate system,[22] and a liquid Ar film deposited on a Pt substrate.[23,24]

In this paper, we report the results of MD simulations of nanosecond laser heating of a Si substrate covered by a Xe overlayer. The simulations are designed to provide a better understanding of the mechanism of the buffer layer ejection in BLALP and to reveal the factors controlling the shapes of the surface features created by the laser patterning. The predictions of the MD simulations are related to the results of experimental analysis of laser patterning in BLALP.

2. COMPUTATIONAL METHOD

The MD simulations are performed for systems consisting of a Xe layer deposited on a Si substrate. The substrate is represented by a slab that has a diamond lattice structure and consists of 5408 Si atoms arranged in eight (001) atomic planes oriented parallel to the surface of the slab. The lateral (parallel to the surface) dimensions of the computational system are 142 Å × 71 Å and periodic boundary conditions are applied in the lateral directions. The Xe buffer layer has a face centered cubic (fcc) structure with (001) planes oriented parallel to the surface of the Si slab. The Xe layers of various thickness, from 16 to 40 monolayers, are used in the simulations. Each monolayer consists of 484 atoms, with the total number of Xe atoms in the layer ranging from 7744 to 19360. The lateral dimensions of the computational system correspond to 26×13 diamond lattice unit cells for the Si substrate and 22×11 fcc unit cells for the Xe overlayer. Each system is thoroughly equilibrated at a temperature of 20 K prior to the beginning of the laser heating. The equilibration results in the formation of a semicoherent interface between the partially dimerized Si (001) face and the Xe overlayer. The MD equations of motion are integrated with the Nordsieck fifth order predictor-corrector algorithm[25] with an integration time step of 5 fs.

The laser heating of the Si substrate is implemented by applying temperature control to the top four atomic layers of the Si slab while keeping the bottom four atomic layers rigid. The temperature of the Si surface is maintained with the Berendsen thermostat method.[26] Two heating regimes are explored in the simulations.

In the first regime, the Si substrate is uniformly heated and the temperature evolution at the Si surface replicates the numerical solution of the one-dimensional heat conduction equation with a source term describing the irradiation by a 5 ns laser pulse. The heat conduction equation is solved for the Si substrate with constant room temperature values of heat capacity, $C_p = 710$ J/(kg K), density, $\rho = 2320$ kg/m^3, thermal conductivity, $k = 150$ W/(m K), and heat diffusion coefficient, $D = k/(\rho C_p) = 9.1 \times 10^{-5}$ m^2/s.[27] An estimation of the amount of thermal energy required for complete vaporization of the Xe overlayers indicates that it is below 1% of the total energy deposited by the laser pulses. Thus, the effect of the heat transfer to the Xe overlayer on the evolution of the surface temperature of the Si substrate is neglected in the solution of the heat diffusion equation. The parameters of the source term are chosen for laser wavelength of

337 nm (optical absorption coefficient of Si is 1.12×10^6 cm^{-1}, ref 27) and the Gaussian temporal profile of the laser pulse. The peak intensities of the Gaussian laser pulses are reached at the time of 5 ns from the beginning of the simulations. The wavelength used in the simulations is shorter than the 532 nm used in the experimental part of the work (see section 3) and has a factor of 170 larger absorption coefficient. As a result, the heating rate of the silicon substrate is faster and, more importantly, the temperature gradient generated in the surface region of the Si substrate by the laser energy deposition is much steeper. The steeper temperature gradient results in a faster cooling, thus limiting the time of the active heat transfer that can contribute to the overlayer removal to less than 20 ns and allowing us to explore different regimes of the overlayer ejection in MD simulations.

The second heating regime is designed to explore the effect of the spatial localization of the laser energy deposition. In this case, the heating is applied to a stripe of the Si substrate, the heated part of the computation cell is maintained at a designated constant temperature for the entire duration of the simulation, 20 ns, and the surface temperature outside the heated stripe is maintained at 0 K (it is found that keeping the temperature of the surface outside the heated stripes at 20 K does not affect the results of the simulations). This heating regime roughly mimics the conditions realized in BLALP, albeit at a much smaller lateral scale.

The interatomic interactions are described by a combination of Stillinger−Weber (SW) and Lennard-Jones (LJ) potentials. The SW potential with the original set of parameters suggested in ref 28 is used for Si−Si interactions. The Xe−Xe and Si−Xe interactions are described by the LJ potential. The parameters $\sigma_{Xe-Xe} = 4.05$ Å and $\varepsilon_{Xe-Xe} = 2.1$ kJ/mol, suggested in ref 29, are chosen for Xe−Xe, with the potential cutoff of 2.5σ used in the simulations. The potential predicts the binding energy of 3.3 ± 0.1 kcal/mol for a surface atom on a (001) face of a Xe crystal, which is close to the value of evaporation energy obtained in multilayer Xe desorption experiments,[30] 3.6 kcal/mol. The parameters for Si−Xe interaction, $\sigma_{Si-Xe} = 3.9$ Å and $\varepsilon_{Si-Xe} = 1.6$ kJ/mol, were fitted in ref 31 to the sum of the van der Waals radii of Si and Xe and to the experimental adsorption energy of Xe on Si(100)-2 × 1 surface, respectively. While being relatively simple, the SW and LJ interatomic potentials provide a good quantitative description of the thermodynamic properties of Si and Xe relevant to the conditions of the simulations. In particular, the heat of vaporization of Xe and the equilibrium melting temperature of Si are both within 5% of the experimental values. An additional bonus is that the phase diagram of Lennard-Jones system is well established,[32−34] providing us with the thermodynamic parameters necessary for interpretation of the results. In particular, the critical temperature, T_c, of LJ Xe is estimated to be 310 K for the potential used in this work.[34]

3. EXPERIMENTAL SETUP

The experimental setup has been described in detail elsewhere.[9,30] Briefly, a standard ultrahigh vacuum chamber at a base pressure of 5×10^{-10} mbar, equipped with Ne$^+$ sputter gun for sample cleaning and a quadrupole mass spectrometer (QMS, VG SX-200) for exposure and coverage determination and calibration, is used in the experiments. In addition, separate Au, Ag, or Ti deposition sources are attached, with in situ quartz microbalance detector for flux calibration measurements. A native

6251

dx.doi.org/10.1021/jp111658w |*J. Phys. Chem. A* 2011, 115, 6250–6259

oxide $SiO_2/Si(100)$ sample is attached via copper rods to a closed cycle helium cryostat (APD) capable of cooling the sample down to 25 K and a heating capability up to 800 K.[30]

In order to perform the laser ablation and patterning measurements, a p-polarized Nd:YAG pulsed laser working at the second harmonic wavelength was employed ($\lambda = 532$ nm, 5 ns pulse duration). The laser power absorbed by the silicon substrate was kept lower than 18 MW/cm^2 to avoid surface damage. In interpretation of the experimental results, we assume complete thermalization between the Si substrate and the thin ($\sim$2.5 nm thick) SiO_2 layer, with no influence of the oxide layer on the heat flow toward the adsorbates. Details of the Xe template formation via laser induced thermal desorption (LITD) and its characterization are given elsewhere.[6−9,35] After patterning the physisorbed Xe, a 12 ± 1 nm thick layer of metal, typically Au or Ag, was deposited on the entire sample. Subsequently, a second uniform pulse strikes the surface, ablating the stripes of the Xe buffer layer remaining on the substrate together with the deposited metal film/clusters and leaving behind the strongly bound metal stripes that are in direct contact with the SiO_2 surface.[9] A 2 ± 1 nm thick layer of Ti was deposited on top of the SiO_2 prior to the metal grating formation. The Ti adhesion layer was found to have no significant effect on the optical properties of the substrate[36] and was necessary to ensure the formation of stable and smooth metallic (Au or Ag) stripes on the $SiO_2/Si(100)$ substrate.[37−40]

4. RESULTS AND DISCUSSION

4.1. MD Simulations of Uniform Laser Heating. In the first series of MD simulations, the Si substrates are uniformly heated by 5 ns laser pulses and the simulations are performed for various values of laser power and three systems where the Xe layers are 16, 32, and 40 monolayer (ML) thick. Two regimes of atomic ejection have been identified in the simulations and are illustrated in Figure 1 for the 16 ML system.

The first regime is realized at low laser powers and corresponds to the intensive evaporation of the Xe overlayer. The mechanism of Xe atoms ejection in this regime is illustrated in Figure 1A, where snapshots from a simulation performed at 12 MW/cm^2 are shown. The heat transfer from the Si substrate to the Xe overlayer results in a gradual heating of the overlayer. By the time of 5.6 ns after the onset of the laser heating (this time corresponds to 0.6 ns after the peak intensity of the laser pulse, see section 2), the temperature of the overlayer is sufficiently high for the onset of melting at the Si−Xe interface and at the free surface of the Xe overlayer. The melting and boiling temperatures of Xe are close to each other (experimental values are 161 and 166 K, respectively[41]) and the surface melting coincides with the beginning of active evaporation. As the temperature of the overlayer continues to increase, the evaporation intensifies (e.g., snapshot for 9.4 ns in Figure 1A) and results in the complete removal of the overlayer after $\sim$15 ns. Note that although the maximum temperature of the Si substrate reaches the value of 485 K at $\sim$6.5 ns, the average temperature of the overlayer does not exceed the level of 204 K, which is $\sim$35% below the critical temperature of the model Xe, 311 K.

A qualitative change in the mechanism of removal of the Xe layer occurs as the laser power exceeds a certain threshold value: It changes from the continuous surface evaporation to the detachment of the entire Xe layer driven by the explosive boiling of a part of the Xe layer adjacent to the Si substrate. This is
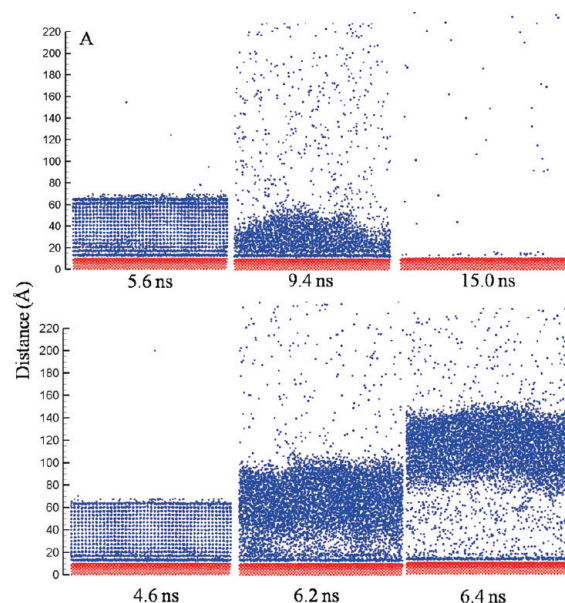

Figure 1. Snapshots taken from MD simulations of laser-induced removal of a Xe overlayer from Si(100) surface. The simulations are performed for 16 ML thick overlayer and laser powers of 12 MW/cm^2 (panel A) and 16 MW/cm^2 (panel B). The Xe atoms in the snapshots are colored blue, the Si atoms are colored red (see text for detailed description of the Si slab dynamics). The simulations in A and B illustrate the two modes of atomic ejection: Continuous evaporation of the overlayer (A) and explosive boiling of the interfacial region leading to the collective ejection (detachment) of the entire layer (B).

illustrated in Figure 1B, where the results are shown for a laser power of 16 MW/cm^2. Similar to the case of lower laser power discussed above, the heat transfer from the Si substrate results in melting and surface evaporation of Xe. The difference, however, is that the temperature of the part of the Xe layers adjacent to the Si substrate reaches the level of $\sim$0.93T_c, resulting in the onset of explosive boiling of the overheated material. The explosive release of vapor phase generates pressure that drives the upper part of the overlayer away from the substrate, as shown in the snapshot for 6.4 ns in Figure 1B. The sharp increase in the vapor nucleation rate in a narrow temperature interval around 0.9T_c has been predicted theoretically based on the classical nucleation theory[42−44] and confirmed in earlier MD simulations.[45] In particular, it has been shown that the incubation period for the onset of the homogeneous boiling of the Lennard-Jones fluid drops from more than a nanosecond down to picoseconds as the temperature increases by $\sim$1% at the threshold for the explosive boiling.[45] Analysis of the simulations illustrated in Figure 1 reveals that the maximum temperature of the Si surface and the adjacent three layers of the Xe overlayer are $T_{Si}^{max} \approx 485$ K and $T_{Xe}^{max} \approx 204$ K (0.65 T_c) at 12 MW/cm^2 and $T_{Si}^{max} \approx 650$ K and $T_{Xe}^{max} \approx 290$ K (0.93 T_c) at 16 MW/cm^2.

The detachment of the overlayer due to the explosive boiling at the Si−Xe interface has been observed for systems with different Xe layer thickness. The time to reach the onset of the explosive boiling and the laser power threshold for the transition from the evaporation mode to the overlayer detachment both increase with increasing thickness of the Xe layer. This is demonstrated in Figure 2, where snapshots from simulations performed for overlayers of three different thicknesses are shown at the onset of explosive boiling and overlayer detachment from

the substrate. For the same laser power of 16 MW/cm^2, the time required to heat up the interfacial part of the Xe overlayer to ~0.9T_c (average temperature is calculated for 3 ML adjacent to the Si substrate) increases from ~6 ns (Figure 2A) up to ~7 ns (Figure 2C) as the thickness of the overlayer increases from 16 to 40 ML.

The thickness dependence of the onset of the explosive boiling in the interfacial region can be explained by the larger total heat capacity of the thicker layers. When the heat flowing through the Si—Xe interface is distributed over a thicker layer, the time required for bringing the temperature of the interfacial region of the Xe overlayer to the threshold temperature for the explosive boiling is longer, as observed in Figure 2. The time required for the thermal equilibration within the overlayer also increases with thickness, leading to the generation of a temperature gradient within the overlayer. Indeed, one can see that the upper part of the 40 ML overlayer shown in Figure 2C still remains in the crystal form while the region adjacent to the Si substrate already experiences the explosive boiling. The observation of the uneven temperature distribution in thick overlayers is consistent with earlier computational results reported for water overlayers on a hot metal surface.[19,20] These studies and the results illustrated in Figure 2 indicate that both the threshold laser power and the time needed to approach the onset of the interfacial boiling reach a saturation with further increase of the overlayer thickness.

The upper parts of the Xe overlayers ejected in the high laser power regime are stabilized by the periodic boundary conditions and retain their flat layered shapes for the duration of the
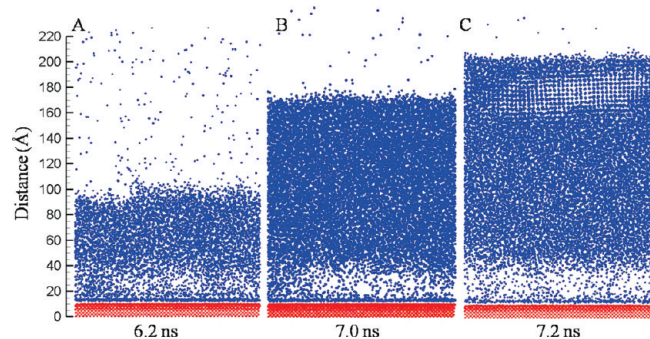

Figure 2. Snapshots from MD simulations of laser-induced removal of Xe overlayers from Si(100) surface. The simulations are performed with the same laser power of 16 MW/cm^2 and three thicknesses of the Xe overlayer: 16 ML (A), 32 ML (B), and 40 ML (C). Atoms in the snapshots are colored in the same way as in Figure 1.
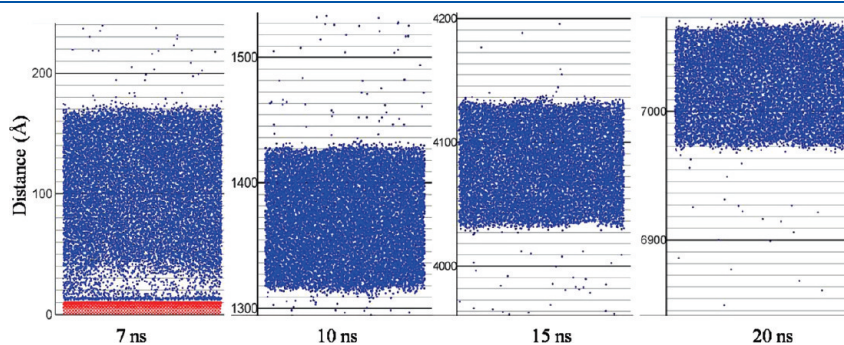
simulations, e.g., Figure 3. Moreover, while the initial heating results in a significant expansion of the ejected Xe slab (from ~100 to ~140 Å in the case shown in Figure 3) the thickness of the slab shrinks again and the density increases with time as the slab cools down due to the extensive evaporation from the top and bottom surfaces of the Xe slab. Note that under experimental conditions, a thin melted film accelerated away from the substrate by the explosive boiling is likely to promptly lose its stability and decompose into individual liquid droplets.

More insight into the energy exchange between the Si substrate and the Xe overlayer can be gained by monitoring the average temperature of Xe atoms during the laser heating process. This evolving temperature, averaged over the entire Xe layer, is compared to that of the Si substrate in Figure 4. There is an incubation time of ~3 ns (somewhat longer for the thicker overlayers) for the beginning of an active heat transfer from the substrate to the Xe slab. This incubation time suggests that the rate of the interfacial energy transfer is slow at low substrate temperatures and has a strong temperature dependence. When the temperature of the Xe slab reaches the melting temperature (at ~5 ns for 16 ML slab and ~5.5 ns for the thicker ones), the transformation of thermal energy into the latent heat of melting modifies the Xe temperature profiles. In the case of the homogeneously heated 16 ML film, melting of the entire layer takes relatively short time and results in a dip in the temperature profile at ~5 ns. The temperature gradients established in the thicker films result in a more gradual melting process and the corresponding decrease in the rates of the temperature rise.

The onset of the explosive boiling in the interfacial region of the Xe overlayer is reflected in sharp drop of the average temperature of the slab. This is due to the transfer of the thermal energy to the heat of explosive vaporization. This drop is more pronounced for the thinner overlayer since the vaporization affects a larger fraction of the overlayer. The explosive boiling pushes the overlayer away from the substrate and drastically decreases the heat transfer from the hot substrate to the ejected part of the overlayer. The active evaporation from the ejected Xe layers continues to cool them for the remaining part of the simulation, up to 20 ns. Although the 16 ML Xe slab reaches the highest temperature in the MD simulations, Figure 4, it also cools down faster than the 32 and 40 ML Xe slabs. Similar behavior, related to the larger heat capacity and less effective evaporative cooling of the thicker slabs, was observed in simulations of water and Ar layers of various thicknesses ejected from hot metal substrates.[19,20,23,24] An observation of the size dependence of the internal temperature of clusters generated in MD simulations of

Figure 3. Snapshots from simulations performed for a system with 32 ML thick Xe overlayer irradiated at a laser power of 16 MW/cm^2. Atoms in the snapshots are colored in the same way as in Figure 1. At the ablation onset, 7 ns, the Xe overlayer expands up to 140 Å. At 10 ns, its thickness is ~120 Å and, at the end of the MD simulation, at 20 ns, the thickness of the overlayer is back to its initial value of ~100 Å, already 700 nm away from the surface.
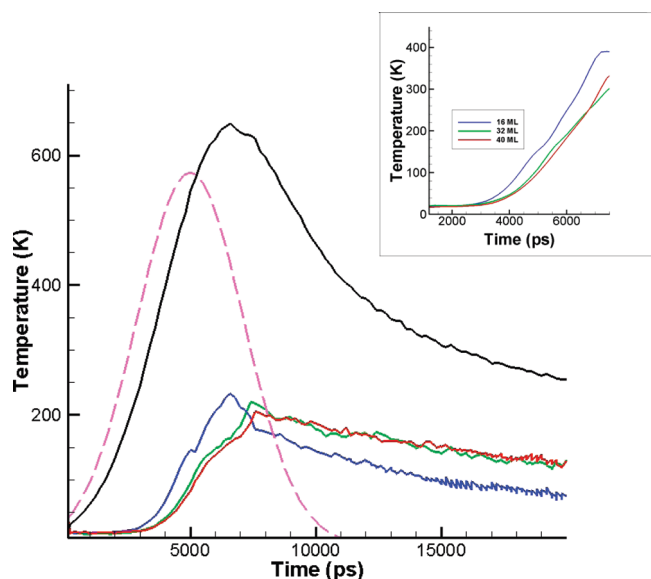
Figure 4. Temperature profiles of the Si surface (black) and Xe overlayers of various thicknesses, 16 ML (blue), 32 ML (green), and 40 ML (red), in simulations performed at laser power of 16 MW/cm². The temperature of the Si surface is controlled by the solution of the one-dimensional heat diffusion equation describing the redistribution of the deposited laser energy within the substrate. The temperature of the Xe overlayers is calculated from the average kinetic energies of all Xe atoms, including the evaporated ones. The dashed line shows the temporal profile of the Gaussian laser pulse. The temperature profiles shown in the inset are calculated for a 3 ML thick slice of the Xe overlayer adjacent to the Si surface up to time of the ablation and detachment of the overlayer from the surface (>7 ns).

laser ablation of molecular targets (larger clusters have higher internal temperature) was also explained by slower evaporative cooling of the larger clusters.[46,47]

An important observation in the simulations discussed above is the slow rate of the energy transfer from the Si substrate heated by the 16 MW/cm² laser pulse up to ∼650 K and the Xe film that heats up to only less than half of that temperature on the nanosecond time scale. The maximum surface temperature is way above the standard desorption temperature (57 K) observed in temperature-programmed desorption (TPD) experiments of Xe from solid surfaces, typically performed at slow heating rates of about 2 K/s and under ultrahigh vacuum conditions.[30,35,48,49] This large difference can be attributed to the difference in the substrate heating rates. Indeed, Xe multilayers ablate from ruthenium surfaces at ∼350 K when the heating is induced by 5 ns pulse irradiation at λ = 532 nm and absorbed laser power of 2.5 MW/cm², while the resistive heating (∼2 K/s) results in multilayer desorption at 57 K.[35] Similarly, the vast difference between the desorption temperature in nanosecond pulsed laser desorption (heating rate of 10^8 K/s) and standard TPD (2 K/s) was observed in MD simulations of water desorption from metallic surfaces.[50] The lack of equilibration between the Si substrate and Xe overlayer on the nanosecond time scale can be attributed to the pronounced difference in the vibrational properties of the two materials. The Debye temperatures are 64 K for Xe and 645 K for Si.[51] The order of magnitude difference in the Debye temperature reflects the large mismatch in the phonon spectra of the two materials that hampers the thermal energy transfer and leads to a high thermal boundary resistance.[52−54]

The fast cooling of the Si surface due to the thermal conduction in the substrate is competing with the slow energy transfer to the volatile overlayer in the nanosecond laser heating experiments. As a result, the high maximum substrate temperatures are required in order to reach the thermodynamic conditions for ablation of the overlayer.

Another manifestation of the weak coupling between the Si substrate and the Xe overlayer is the presence of Xe atoms on the Si surface even at temperatures above the ablation threshold, e.g., snapshots for 6.4 ns in Figure 1B and for 7.2 ns in Figure 2. The coverage of the Si surface by Xe is defined by the balance between the adsorption of atoms evaporating from the departing Xe layer and colliding with the Si surface and the thermal desorption due to the energy transfer from the hot Si surface. As the Xe slab moves further away from the substrate and the density of Xe atoms near the substrate decreases, this balance tilts toward desorption and eventually results in the formation of Xe-free Si substrate.

Once the thermal energy is transferred from the heated Si substrate to the Xe layer, the question arises how rapid is the heat flow and redistribution within the Xe overlayer. This question can be addressed by calculating the temperature profiles within the Xe overlayer at different times during the simulations. The temperature profiles are calculated by dividing the Xe overlayer into 1.4 nm thick slices (correspond to 3 ML of Xe in the initial system) and evaluating the temperature of each slice from the average kinetic energy of the atoms. Analysis of the temperature profiles indicates that temperature gradients develop along the z-direction away from the substrate and the difference between the temperatures of the top and bottom parts of the Xe overlayers is increasing with increasing thickness of the overlayers.

An example of the evolving temperature distribution in the Xe overlayer is shown in Figure 5 for a simulation performed for a system with 40 ML thick Xe overlayer irradiated at a laser power of 16 MW/cm². At 3 ns from the onset of the laser pulse (Figure 5A), the temperature of the Si surface is 245 K but the transfer of the thermal energy to the Xe overlayer has been very limited and the temperature of the overlayer remains below 50 K throughout the depth of the overlayer. At 5 ns (Figure 5B), the Si surface temperature is already at 545 K, which is ∼100 K lower than its peak value. By this time, the thermal energy flow from the Si surface has increased the temperature of the bottom part of the Xe overlayer above 100 K, while the upper layers are still below 80 K. At 6.4 ns (Figure 5C), the temperature of the Si surface is practically at its peak value of 645 K (see Figure 4). The temperature in the ∼6.5 nm part of the Xe overlayer exceeds the melting temperature, leading to the melting of the lower part of the overlayer. The bottom slice of the Xe slab is reaching the temperature of 224 K ($0.72T_c$), which is still below the threshold for the onset of explosive boiling. The temperature for the onset of the explosive boiling (∼$0.9T_c$ or 280 K) is reached only by ∼7 ns (see inset in Figure 4), leading to the fast release of the vapor phase and lift off (or ablation) of the overlayer. A postablation snapshot at 7.2 ns (Figure 5D) reveals melting of most of the Xe overlayer, with only a small region in the top part of the overlayer retaining its crystal structure. Note that the explosive boiling of the region adjacent to the Si substrate provides an efficient cooling mechanism. As a result, the maximum temperature in the Xe overlayer shifts a few nanometers up from the bottom surface of the ejected overlayer.

4.2. MD Simulations of Localized Laser Heating. In order to investigate the effect of the spatial localization of the laser energy

6254

dx.doi.org/10.1021/jp111658w |*J. Phys. Chem. A* 2011, 115, 6250–6259
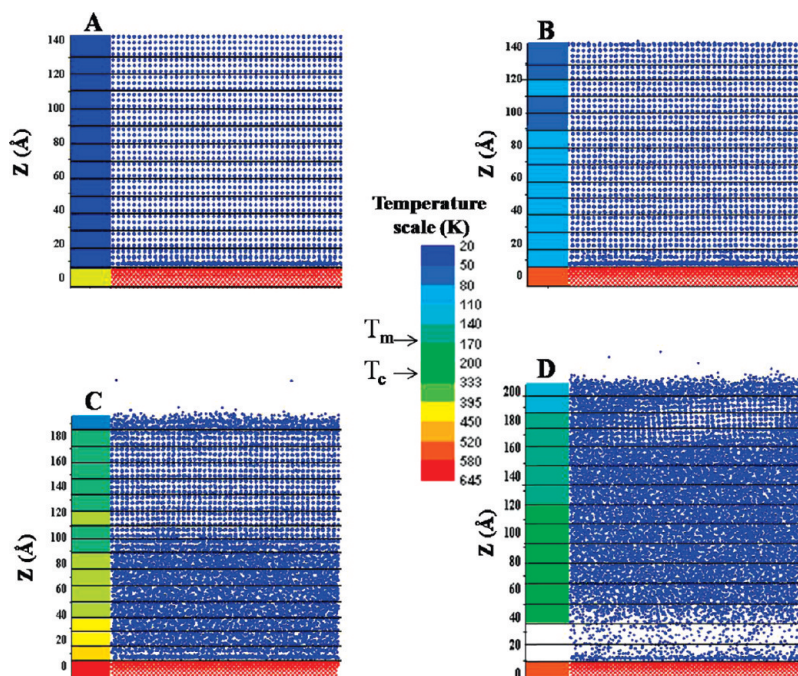
Figure 5. Snapshots and temperature profiles (shown by color code to the left of the corresponding snapshots) for MD simulation performed for a system with 40 ML thick Xe overlayer irradiated at a laser power of 16 MW/cm^2. The temperature is calculated for 1.4 nm slices of the system outlined by the horizontal black lines. The snapshots and temperature distributions are shown for 3 ns (A), 5 ns (B), 6.4 ns (C), and 7.2 ns (D) after the start of the simulation. Atoms in the snapshots are colored in the same way as in Figure 1.
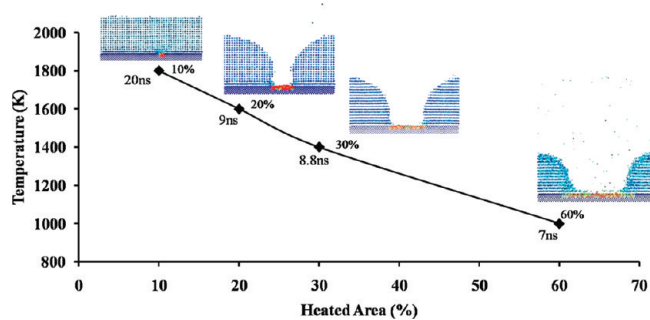

Figure 6. The dependence of the surface temperature required for complete ablation of a part of the Xe overlayer located above the heated stripe of the Si substrate within the time of ∼10 ns. Combinations of the temperature and minimum heating duration required for the ablation are shown for stripes with the widths of 20, 30, and 60% of the computational cell. Longer heating duration at lower temperatures results in similar ablation profile. An additional point is shown for the smallest stripe of 10% of the computational cell, where no ablation is observed within 20 ns at a temperature of the strip of 1800 K. The snapshots taken at the end of the corresponding simulations are shown in the plot.

deposition, realized in laser interference experiments, we performed a separate set of MD simulations where the heating is laterally confined to a fraction of the Si surface. In each of these simulations, the temperature control is applied to a stripe of the Si substrate in the middle of the computational system. The temperature of the stripe is maintained constant over the entire 20 ns simulation time, with the rest of the Si substrate kept at 0 K. The simulations are performed for heated regions that are 10, 20, 30, and 60% of the total width of the computational cell, which corresponds to 14, 28, 47, and 85 Å, respectively.

The results of the simulations suggest that, in order to reach the complete ablation of a fraction of the Xe overlayer located above the heated area of the Si substrate within the duration of the simulations (20 ns), the temperature of the heated stripes should be substantially higher than the maximum temperature of the Si surface reached in the simulations of homogeneous pulsed heating discussed in the previous section. Moreover, decreasing the size of the heated stripe results in a substantial increase in the temperature of the heated stripe (laser power) and/or the heating duration required for the complete spatially selective ablation, Figure 6. The heating of 30% and 20% of the surface requires a minimum of 8.4 and 9 ns at temperatures of 1400 and 1600 K, respectively. The heating of 10% or less of the substrate does not result in desorption of Xe within 20 ns even at a temperature of 1800 K that exceeds the melting temperature of the SW silicon (1677 K).[55,56]

The high temperature required for the spatially selective ablation of the overlayer can be explained by (1) the efficient lateral heat exchange from the heated part of the Xe area to the surrounding colder Xe regions and (2) the stabilizing effect of the colder regions that hold the heated part of the Xe overlayer in place and prevent its separation from the Si substrate. The latter effect makes the intense and continuous evaporation of Xe atoms to be the only mechanism of the overlayer removal in the range of the simulation parameters considered in this work. Unlike the laterally uniform heating, where above a certain laser power (surface temperature) a lift off of the overlayer driven by the explosive boiling takes over, the evaporation mechanism is responsible for the selective overlayer removal (patterning) even at temperatures approaching the threshold for substrate melting/ damage, e.g., Figure 7. We would like to note that a transition to the regime of explosive boiling has been observed in simulations
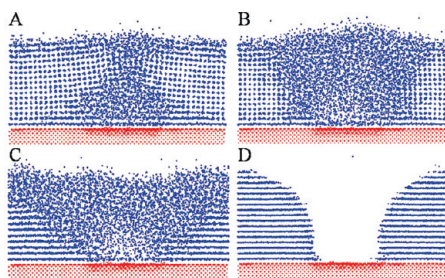
Figure 7. Snapshots from a simulation of selective ablation of a 16 ML Xe overlayer. A 30% part of the Si surface is kept at a fixed temperature of 1400 K for 20 ns, the entire duration of the MD simulation. The snapshots are for 0.4 ns (A), 0.8 ns (B), 4 ns (C), and 8.8 ns (D) of heating. Atoms in the snapshots are colored in the same way as in Figure 1.

Figure 8. Laser ablation of Xe coverage grating. Ratio of the first-order optical diffraction intensity, recorded after and before the second (uniform) pulse is applied to the Xe-covered silicon substrate, is plotted vs power of the second pulse. The curves represent series of experiments performed for 80 ML (black) and 160 ML (red) Xe layers. In both cases, the power of the laser used for the grating formation was maintained at 13.8 MW/cm^2.

of localized heating performed at higher temperatures, in the range of 4000−5000 K for a heated area of 25% (not shown). In these simulations, the generation and expansion of vapor bubbles above the heated parts of the substrate resulted in the ejection of large Xe droplets. The localized heating in these simulations also produced a substantial damage to the Si substrate.

4.3. Fractional Ablation Experiments. In order to establish correlations between the results of the MD simulations and experimental observations, a series of measurements aimed at establishing the threshold laser power for removal of Xe over-layer were performed. The scheme for the experimental mea-surements was based on generation of Xe coverage grating on a SiO$_2$/Si(100) surface, as explained in detail in Section 3 and refs 9, 11, and 35. First-order optical diffraction was generated and recorded from the resulting Xe coverage grating when continu-ously irradiated by a 5 mW continuous wave HeNe laser. A second, uniform laser pulse was then applied at gradually higher power in order to determine the minimum laser power that leads to the removal of the modulated Xe coverage grating, resulting in instantaneous removal of the optical diffraction signal.

In order to check the effect of the layer thickness on the ablation threshold, the same procedure was applied to Xe over-layers, 80 and 160 ML thick. The ablating laser power was gradually increased from 6.6 to 16.7 MW/cm^2. Laser powers of 13.8 and 16.7 MW/cm^2 were found necessary for reaching complete ablation of 80 and 160 ML of Xe, respectively, as demonstrated in Figure 8. These values of laser power corre-spond to (calculated) surface peak temperatures of 202 K at 13.8 MW/cm^2 and 244 K for 16.7 MW/cm^2. Thus, in agreement with the predictions of MD simulations, the minimum power required for overlayer removal is indeed sensitive to the Xe layer thickness and increases with increasing thickness.

The substantial difference between the surface temperature at the threshold for the Xe overlayer removal predicted in the simulations and estimated for the experimental conditions can be explained by the difference in the laser energy deposition in the Si substrate. At the excitation wavelength used in the experiments, $\lambda = 532$ nm, Si absorption coefficient is $\alpha = 6730$ cm^{-1} and the corresponding optical penetration depth is $L_p = 1/\alpha = 1.5 \times 10^{-4}$ cm. This value is 170 times larger than the penetration depth $L_p = 8.97 \times 10^{-7}$ cm at the wavelength used in MD simulations, $\lambda = 337$ nm. The effect of deeper optical penetration under the experimental conditions is 2-fold. On one hand, it results in a lower energy density absorbed at the surface region which reduces the maximum surface temperature. On the other
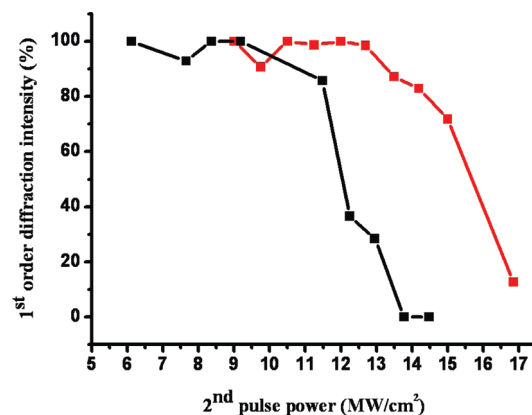
hand, it generates smaller temperature gradients within the Si substrate and creates the conditions for much slower cooling of the surface. These two consequences of longer penetration depth have opposite effects on the removal of the Xe overlayer, thus providing a hint for explaining why, despite the large difference in the maximum surface temperatures, the power threshold values for the overlayer removal are similar in the simulations and experiments. The difference in the temperature profiles gener-ated at the surface of clean (without Xe overlayer) Si substrate by irradiation at the two laser wavelengths is illustrated in Figure 9. The slower cooling of the Si surface in the case of 532 nm irradiation allows for a longer time of thermal energy transfer to the Xe overlayer. We note that the peak temperature predicted for the grating formation conditions in both simulations (at $\lambda = 337$) and experiments (at $\lambda = 532$ nm) are significantly higher than the Xe multilayer peak desorption temperature obtained by standard (slow heating rate, 2 K/s) TPD measurements, 57 K (ref 35).

We cannot quantitatively compare the laser power thresholds obtained for partial ablation in the MD simulations to that determined experimentally. This is due to the size of the ablated area in the MD simulation being only 14−48 Å wide for the 10−60% fractional heating. These limited sizes (dictated by the computationally demanding nature of atomic-level modeling) are 3 orders of magnitude narrower than the experimental stripes, resulting in significantly more efficient lateral heat redistribution within the Xe overlayer. We do predict however, that the wide ablated area in the experiment is well represented by the explo-sive boiling mechanism discussed in section 4.1. Indeed, the effect of the cooling by heat transfer to the surrounding cold regions that is so effective in the narrow troughs used in the MD simulations are expected to be negligible under experimental conditions. Nevertheless, it may be instructive to relate, at a qualitative level, the shapes of the Xe troughs obtained in experiments and in MD simulations.

Experimentally, one can imprint the profile of the modulated Xe coverage (grating) by exposing the Xe pattern to 12−15 nm thick layer of Ag, deposited in vacuum. Following the second uniform laser pulse, Ag stripes are left behind as explained in
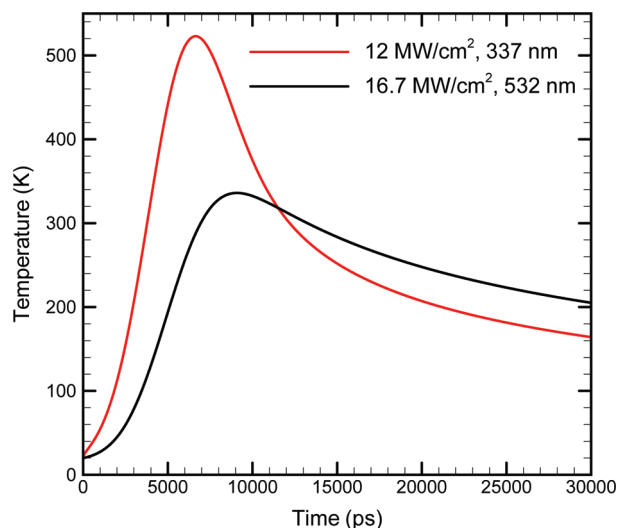
Figure 9. The surface temperature profiles predicted by solving one-dimensional heat conduction equation for clean (without Xe overlayer) Si substrate irradiated by a 5 ns laser pulse. The results are shown for the following values of laser wavelength and laser power: 337 nm and 12 MW/cm^2 (red curve) and 532 nm and 16.7 MW/cm^2 (black curve).
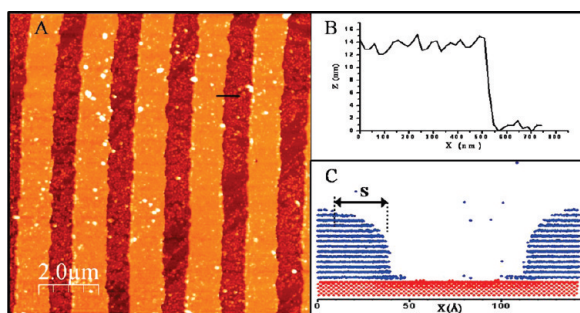

Figure 10. The results of laser patterning experiments (panels A and B) and MD simulations of selective ablation of a Xe overlayer (panel C). The laser patterning experiments are demonstrated via a 12 nm thick Ag film deposited on top of modulated Xe film on Ti/SiO$_2$ surface. The interfering laser was operated at a wavelength of 532 nm and laser power of 13.0 MW/cm^2. Panel B shows an AFM line scan taken along the black line shown in the top-right part of the image in panel A. A snapshot from the MD simulations of the selective heating (60% heated, see text) to 1000 K is shown in panel C, with width of the trough(s) revealing the level of steepness obtained at the edges of the ablated Xe stripes.

more detail in the Experimental Section and refs 6 and 57. A demonstration of such a lift-off experiment for a Ag/Ti/SiO$_2$/Si system is presented in Figure 10. We have previously demonstrated[8,9,57] that by tuning the ablation laser power, one can determine and control the fractional Xe layer width or the fraction of Xe layer to be ablated. The wider part of the sinusoidal heating profile exceeds the ablation threshold as the laser power increases. At 13.0 MW/cm^2, the power used in the experiment illustrated in Figure 10, 55% of the Xe layer has ablated.

The profiles of Xe troughs obtained experimentally and in the MD simulations of the selective heating have been qualitatively compared and appreciated via the width "S" in Figure 10C obtained from the MD simulations and by the edge of the experimental Ag profiles. The ablated Xe area in the simulations (60% of the slab) models the empty trough "mold" where the

metal atoms are deposited in the experiment. The slopes of the metal-line edge are expected to roughly correspond to the steepness of the Xe template trough profiles. Experimental "S" of about 50 nm is obtained from interference of two laser beams at 532 nm, while in the MD model a Xe "S" edge of 30 Å was obtained from 60% heated area. The simulated value of "S" is not expected to change in a significant way if we would have extended the lateral dimensions of the Xe slab. Due to the significant difference in length scales between the MD simulations and experiments, the comparison between the two is limited to qualitative level.

5. CONCLUSIONS

The physical mechanisms of laser-induced selective removal of a Xe overlayer from a Si substrate are investigated in series of MD simulations and related to the results of experimental analysis of surface features generated in a recently developed buffer layer assisted laser patterning technique. The results of the simulations performed for Si substrates uniformly heated by 5 ns laser pulses reveal two regimes of atomic ejection. At low laser powers and small thicknesses of the Xe overlayer, a gradual heat transfer from the substrate heats up the overlayer, leading to the intensive evaporation of the overlayer. At higher laser powers, the continuous surface evaporation changes into the detachment of the entire Xe layer driven by the explosive boiling of a part of the Xe layer adjacent to the Si substrate. In this second regime, the heat transfer from the substrate results in the temperature gradient established within the overlayer. The temperature of the hot part of the overlayer adjacent to the substrate eventually reaches the limit of thermodynamic stability of the overheated fluid ($\sim 0.9 T_c$) and triggers the explosive boiling in the interfacial region. The explosive release of vapor phase generates pressure that drives the upper (and colder) part of the overlayer away from the substrate. The time of the onset of the explosive boiling and the laser power threshold for the transition from the evaporation regime to the explosive boiling and detachment of the overlayer both increase as the thickness of the Xe layer increases from 16 to 40 ML. The regime of the explosive boiling and detachment of the overlayer is preferable for high-quality patterning in the BLALP technique as it is likely to be more effective (compared to the evaporation) in clean removal of the metal film residing on the overlayer.[8,9]

The large mismatch in the phonon spectra of the substrate (Si) and overlayer (Xe) materials is responsible for low rates of the heat flow from the substrate to the overlayer. As a result, the temperature at the two sides of the Si—Xe interface remains very different at the nanosecond time scale, with the maximum temperature in the Xe overlayer being less than half of that of the Si substrate. In the simulations of the selective heating of a stripe of the silicon substrate, the lateral heat transfer to the colder regions of the Xe overlayer and the stabilizing effect of bonding to the colder regions that hold the heated part of the Xe overlayer in place and prevent its separation from the Si substrate are identified as two factors that substantially increase the substrate temperature required for achieving the spatially selective ablation of the overlayer.

The predictions of the MD simulations are related to the experimental measurements that establish the threshold laser power for removal of Xe overlayers of different thickness. In agreement with computational results, the peak substrate temperatures at the thresholds for the overlayer removal are found to

be substantially higher than the overlayer desorption temperature measured in slow heating rate TPD experiments. The maximum temperatures in experiments are smaller than those in the simulations due to the smaller simulated laser absorption depth which leads to the faster cooling of the Si surface following laser excitation.

Despite the difference in the length scales, the MD simulations provide important qualitative information and atomic level insight into the formation of experimentally observed shapes of metallic stripes generated by BLALP.

■ AUTHOR INFORMATION

Corresponding Author

*E-mail: asscher@chem.ch.huji.ac.il.

■ REFERENCES

(1) Imen, K.; Lee, S. J.; Allen, S. D. Laser-assisted micron scale particle removal. *Appl. Phys. Lett.* **1991**, *58*, 203–205.

(2) Zapka, W.; Ziemlich, W.; Tam, A. C. Laser cleaning techniques for removal of surface particulates. *J. Appl. Phys.* **1992**, *71*, 3515–3523.

(3) Nelson, R. W.; Rainbow, M. J.; Lohr, D. E.; Williams, P. Volatilization of high molecular weight DNA by pulsed laser ablation of frozen aqueous solutions. *Science* **1989**, *246*, 1585–1587.

(4) Williams, P. Time of flight mass spectrometry of DNA laser-ablated from frozen aqueous solutions: applications to the Human Genome Project. *Int. J. Mass. Spectrom.* **1994**, *131*, 73–96.

(5) Berry, J. I.; Sun, S. X.; Dou, Y. S.; Wucher, A.; Winograd, N. Laser desorption and imaging of proteins from ice via UV femtosecond laser pulses. *Anal. Chem.* **2003**, *75*, 5146–5151.

(6) Kerner, G.; Asscher, M. Laser patterning of metallic films via buffer layer. *Surf. Sci.* **2004**, *557*, 5–12.

(7) Kerner, G.; Horowitz, Y.; Asscher, M. Diffusion of buffer layer assisted grown gold nanoclusters on Ru(100) and p(1 × 2)-O/Ru(100) surfaces. *J. Phys. Chem. B* **2005**, *109*, 4545–4553.

(8) Kerner, G.; Asscher, M. Buffer layer assisted laser patterning of metals on surfaces. *Nano Lett.* **2004**, *4*, 1433–1437.

(9) Kerner, G.; Stein, O.; Asscher, M. Patterning thin metallic film via laser structured weakly bound template. *Surf. Sci.* **2006**, *600*, 2091–2095.

(10) Zhu, X. D.; Rasing, Th.; Shen, Y. R. Surface diffusion of Co on Ni(111) studied by diffraction of optical second-harmonic generation off a monolayer grating. *Phys. Rev. Lett.* **1988**, *61*, 2883–2885.

(11) Williams, P. A.; Reider, G. A.; Li, L.; Höfer, U.; Suzuki, T.; Heinz, T. F. Physisorbed template for spatial patterning of adsorbates. *Phys. Rev. Lett.* **1997**, *79*, 3459–3462.

(12) Weaver, J. H.; Waddill, G. D. Cluster assembly of interfaces: Nanoscale engineering. *Science* **1991**, *251*, 1444–1451.

(13) Antonov, V. N.; Palmer, J. S.; Waggoner, P. S.; Bhatti, A. S.; Weaver, J. H. Nanoparticle diffusion on desorbing solids: The role of elementary excitations in buffer-layer-assisted growth. *Phys. Rev. B* **2004**, *70*, 045406.

(14) Kudryashov, S. I.; Allen, S. D. Optical transmission measurements of explosive boiling and liftoff of a layer of micron-scale water droplets from a KrF laser-heated Si substrate. *J. Appl. Phys.* **2003**, *93*, 4306–4308.

(15) Kudryashov, S. I.; Allen, S. D. Submicrosecond dynamics of water explosive boiling and lift-off from laser-heated silicon surfaces. *J. Appl. Phys.* **2006**, *100*, 104908.

(16) Lang, F.; Leiderer, P. Liquid—vapour phase transitions at interfaces: sub-nanosecond investigations by monitoring the ejection of thin liquid films. *New J. Phys.* **2006**, *8*, 14.

(17) Frank, P.; Graf, J.; Lang, F.; Boneberg, J.; Leiderer, P. Laser-induced film ejection at interfaces: Comparison of the dynamics of liquid and solid films. *Appl. Phys. A: Mater. Sci. Process.* **2010**, *101*, 7–11.

(18) Samokhin, A. A. Estimate of pressure produced during explosive boiling of a liquid film on a substrate heated by laser pulses. *Quantum Electron.* **2006**, *36*, 684–686.

(19) Dou, Y.; Zhigilei, L. V.; Winograd, N.; Garrison, B. J. Explosive boiling of water films adjacent to heated surfaces: A microscopic description. *J. Phys. Chem. A* **2001**, *105*, 2748–2755.

(20) Dou, Y.; Zhigilei, L. V.; Postawa, Z.; Winograd, N.; Garrison, B. J. Thickness effects of water overlayer on its explosive evaporation at heated metal surfaces. *Nucl. Instrum. Methods Phys. Res., Sect. B* **2001**, *180*, 105–111.

(21) Dou, Y.; Winograd, N.; Garrison, B. J.; Zhigilei, L. V. Substrate-assisted laser-initiated ejection of proteins embedded in water films. *J. Phys. Chem. B* **2003**, *107*, 2362–2365.

(22) Smith, K. M.; Hussaini, M. Y.; Gelb, L. D.; Allen, S. D. Modeling laser-assisted particle removal using molecular dynamics. *Appl. Phys. A: Mater. Sci. Process.* **2003**, *77*, 877–882.

(23) Gu, X.; Urbassek, H. M. Atomic dynamics of explosive boiling of liquid-argon films. *Appl. Phys. B: Laser Opt.* **2005**, *81*, 675–679.

(24) Gu, X.; Urbassek, H. M. Laser-induced desorption of overlayer films off a heated metal substrate. *Appl. Surf. Sci.* **2007**, *253*, 4142–4149.

(25) Allen, M. P.; Tildesley, D. J. *Computer Simulation of Liquids*; Clarendon Press: Oxford, 1987.

(26) Berendsen, H. J. C.; Postma, J. P. M.; van Gunsteren, W. F.; DiNola, A.; Haak, J. R. Molecular dynamics with coupling to an external bath. *J. Chem. Phys.* **1984**, *81*, 3684–3690.

(27) Bäuerle, D. *Laser Processing and Chemistry*; Springer: Berlin, 2000.

(28) Stillinger, F. H.; Weber, T. A. Computer simulation of local order in condensed phases of silicon. *Phys. Rev. B* **1985**, *31*, 5262–5271.

(29) Matyushov, D. V.; Schmid, R. Calculation of Lennard-Jones energies of molecular fluids. *J. Chem. Phys.* **1996**, *104*, 8627–8638.

(30) Stein, O.; Asscher, M. Adsorption of H_2O, CO_2 and Xe on soft surfaces. *J. Phys. Chem. B* **2008**, *112*, 3955–3962.

(31) Utrera, L.; Ramírez, R. Molecular dynamics simulation of Xe diffusion on the Si(100)-2 × 1 surface. *J. Chem. Phys.* **1992**, *96*, 7838–7847.

(32) Lotfi, A.; Vrabec, J.; Fischer, J. Vapour liquid equilibria of the Lennard-Jones fluid from the NpT plus test particle method. *Mol. Phys.* **1992**, *76*, 1319–1333.

(33) Smit, B. Phase diagrams of Lennard-Jones fluids. *J. Chem. Phys.* **1992**, *96*, 8639–8640.

(34) Finn, J. E.; Monson, P. A. Prewetting at a fluid—solid interface via Monte Carlo simulation. *Phys. Rev. A* **1989**, *39*, 6402–6408.

(35) Kerner, G.; Stein, O.; Lilach, Y.; Asscher, M. Sublimative desorption of xenon from Ru(100). *Phys. Rev. B* **2005**, *71*, 205414.

(36) Bentini, G.; Cohen, C.; Desalvo, A.; Drigo, A. V. Laser annealing of damaged silicon covered with a metal film: test for epitaxial growth from the melt. *Phys. Rev. Lett.* **1981**, *46*, 156–159.

(37) Bauer, R. S.; Bachrach, R. Z.; Brillson, L. J. Au and Al interface reactions with SiO_2. *Appl. Phys. Lett.* **1980**, *37*, 1006–1008.

(38) George, M. A.; Bao, Q. C.; Sorensen, I. W.; Glaunsinger, W. S.; Thundat, T. Thermally induced changes in the resistance, microstructure, and adhesion of thin gold films on Si/SiO$_2$ substrates. *J. Vac. Sci. Technol., A* **1990**, *8*, 1491–1497.

(39) Xu, X.; Goodman, D. W. Metal deposition onto oxides: An unusual low initial sticking probability for copper on SiO_2. *Appl. Phys. Lett.* **1992**, *61*, 1799–1801.

(40) Camacho-López, S.; Evans, R.; Escobar-Alarcón, L.; Camacho-López, M. A. Polarization-dependent single-beam laser-induced grating-like effects on titanium films. *Appl. Surf. Sci.* **2008**, *255*, 3028–3032.

(41) *CRC Handbook of Chemistry and Physics*, 63rd ed.; CRC Press: Boca Raton, FL, 1982—1983.

(42) Martynyuk, M. M. *Sov. Phys. Tech. Phys.* **1976**, *21*, 430.

(43) Miotello, A.; Kelly, R. *Appl. Phys. A: Mater. Sci. Process.* **1999**, *69*, S67.

(44) Bulgakova, N. M.; Bulgakov, A. V. *Appl. Phys. A: Mater. Sci. Process.* **2001**, *73*, 199.

(45) Garrison, B. J.; Itina, T. E.; Zhigilei, L. V. The limit of overheating and the threshold behavior in laser ablation. *Phys. Rev. E* **2003**, *68*, 041501.

(46) Zhigilei, L. V.; Garrison, B. J. Microscopic mechanisms of laser ablation of organic solids in the thermal and stress confinement irradiation regimes. *J. Appl. Phys.* **2000**, *88*, 1281–1298.

(47) Zhigilei, L. V. Dynamics of the plume formation and parameters of the ejected clusters in short-pulse laser ablation. *Appl. Phys. A: Mater. Sci. Process.* **2003**, *76*, 339–350.

(48) Bartha, J. W.; Barjenbruch, U.; Henzler, M. Thermal desorption spectroscopy of Xe at the Si(111) as a local probe for surface structures. *J. Vac. Sci. Technol., A* **1985**, *3*, 1588–1591.

(49) Guo, H.; Zaera, F. Xenon as a probe for minority sites on solid surfaces. *Nat. Mater.* **2006**, *5*, 489–493.

(50) Lilach, Y.; Buch, V.; Asscher, M. Formation and dynamics of water clusters on Ru(001). *J. Chem. Phys.* **2003**, *119*, 11899–11905.

(51) Kittel, C. *Introduction to Solid State Physics*; J. Wiley & Sons Inc.: New York, 1996.

(52) Swartz, E. T.; Pohl, R. O. Thermal boundary resistance. *Rev. Mod. Phys.* **1989**, *61*, 605–667.

(53) Swartz, E. T.; Pohl, R. O. Thermal resistance at interfaces. *Appl. Phys. Lett.* **1987**, *51*, 2200–2202.

(54) Stevens, R. J.; Zhigilei, L. V.; Norris, P. M. Effects of temperature and disorder on thermal boundary conductance at solid—solid interfaces: Nonequilibrium molecular dynamics simulations. *Int. J. Heat Mass Transfer* **2007**, *50*, 3977–3989.

(55) Buta, D.; Asta, M.; Hoyt, J. J. Kinetic coefficient of steps at the Si(111) crystal-melt interface from molecular dynamics simulations. *J. Chem. Phys.* **2007**, *127*, 074703.

(56) Dongare, A. M.; Neurock, M.; Zhigilei, L. V. Angular-dependent embedded atom method potential for atomistic simulations of metal-covalent systems. *Phys. Rev. B* **2009**, *80*, 184106.

(57) Kerner, G.; Stein, O.; Asscher, M. Physisorbed buffer layer as a template for pulsed laser patterning of metallic thin films: an alternative approach for photolithography. *Proc. SPIE* **2004**, *5513*, 128–136.